maps and the phosphoamino acid analysis were done as described (*30*).
10. S. J. Moss, T. G. Smart, C. D. Blackstone, R. L. Huganir, unpublished observations.
11. M. D. Uhler *et al.*, *Proc. Natl. Acad. Sci. U.S.A.* **83**, 1300 (1986).
12. S. J. Moss, C. A. Doherty, R. L. Huganir, *J. Biol. Chem.* **267**, 14470 (1992).
13. The HEK293 cells were maintained as described (*8*, *15*). Recordings were made at 25°C from cells superfused with a Krebs solution containing 5 mM Hepes (pH 7.4), 140 mM NaCl, 4.7 mM KCl, 1.2 mM $MgCl_2$, 2.5 mM $CaCl_2$, and 11 mM glucose. Whole-cell recordings were performed with patch pipettes (1 to 5 megohms) containing 10 mM Hepes (pH 7.1), 140 mM KCl, 2 mM $MgCl_2$, 1 mM $CaCl_2$, 11 mM EGTA, and 2 mM adenosine triphosphate. Drugs and normal Krebs were applied to the HEK293 cells and neurons with a rapid perfusion system consisting of a multibarreled electrode made from Quad glass tubing (Clarks Electromedical, Reading, UK) that was positioned within 50 to 100 μm of the cell. Solution exchange with this perfusion system occurred in ~4 ms. The HEK293 cells were used for recording 48 hours after transfection and had resting potentials of −30 to −60 mV. Transfection with wild-type or mutant cDNAs was performed on different cultures of HEK293 cells derived from the same parent colony. As a result of the variation in transfection efficiency, the amplitudes of GABA currents recorded with both the wild-type and the mutant GABA receptors in the absence of cAMP or PKA were quite variable between cells. Comparison of the GABA currents recorded from 29 to 45 cells transfected with either the wild-type or mutant cDNAs for the $\alpha_1\beta_1$ or $\alpha_1\beta_1\gamma_2$ combinations in the absence of cAMP, PKA, or Cα did not reveal any significant differences between their response amplitudes or kinetics. Voltage-clamp currents were recorded with a List (Darmstadt, Germany) EPC7 amplifier, displayed on a Brush-Gould (London) ink-jet pen recorder (2400S), and stored on a Racal (Southampton, UK) store 4DS tape recorder (direct current to 5 kHz). Neurons were cultured from rat superior cervical ganglia of embryonic day 21 (E21) animals as described (*16*). Neurons were used 2 to 4 days after dissociation and had membrane potentials of −50 to −70 mV and action potential amplitudes of 80 to 95 mV. Recordings were made from neurons as described above.
14. T. A. Verdoorn, A. Draguhn, S. Ymer, P. H. Seeburg, B. Sakmann, *Neuron* **4**, 919 (1990).
15. T. G. Smart, S. J. Moss, X. Xie, R. L. Huganir, *Brit. J. Pharmacol.* **103**, 1837 (1991).
16. T. G. Smart, *J. Physiol. (London)* **447**, 587 (1992).
17. A. Draguhn, T. A. Verdoorn, M. Ewert, P. H. Seeburg, B. Sakmann, *Neuron* **5**, 781 (1990).
18. N. J. Leidenheimer, M. D. Browning, R. A. Harris, *Trends Pharmacol. Sci.* **12**, 84 (1991).
19. M. D. Browning, M. Bureau, E. M. Dudek, R. W. Olsen, *Proc. Natl. Acad. Sci. U.S.A.* **87**, 1315 (1990).
20. E. F. Kirkness, C. F. Bovenkerk, T. Ueda, A. J. Turner, *Biochem. J.* **259**, 613 (1989).
21. N. J. Leidenheimer *et al.*, *J. Neurochem.* **57**, 722 (1991).
22. N. M. Porter, R. E. Twyman, M. D. Uhler, R. L. MacDonald, *Neuron* **5**, 789 (1990).
23. E. Sigel and R. Bauer, *Proc. Natl. Acad. Sci. U.S.A.* **85**, 6192 (1988).
24. F. M. Sessler *et al.*, *Brain Res.* **499**, 27 (1989).
25. M. K. Ticku and A. K. Mehta, *Mol. Pharmacol.* **38**, 719 (1990).
26. R. L. Huganir, A. H. Delcour, P. Greengard, G. P. Hess, *Nature* **321**, 774 (1986); J. F. Hopfield, D. W. Tank, P. Greengard, R. L. Huganir, *ibid.* **336**, 677 (1988).
27. P. Kofuji, J. B. Wang, S. J. Moss, R. L. Huganir, D. R. Burt, *J. Neurochem.* **56**, 713 (1991).
28. J. B. Wang *et al.*, *J. Mol. Neurosci.*, in press.
29. T. A. Kunkel, J. D. Roberts, D. L. Zabour, *Methods Enzymol.* **154**, 367 (1987).
30. R. L. Huganir, K. Miles, P. Greengard, *Proc. Natl. Acad. Sci. U.S.A.* **81**, 6968 (1984).
31. Supported by the Howard Hughes Medical Institute, the Medical Research Council (United Kingdom), and the Wellcome Trust. We thank M. D. Uhler (University of Michigan) for the cDNA clones of the catalytic subunit of the cAMP-dependent protein kinase and L. Raymond for critical review of the manuscript.

19 March 1992; accepted 11 June 1992

Neuronal Domains in Developing Neocortex

Rafael Yuste,* Alejandro Peinado, Lawrence C. Katz

The mammalian neocortex consists of a mosaic of columnar units whose development is poorly understood. Optical recordings of brain slices labeled with the fluorescent calcium indicator fura-2 revealed that the neonatal rat cortex was partitioned into distinct domains of spontaneously coactive neurons. In tangential slices, these domains were 50 to 120 micrometers in diameter; in coronal slices they spanned several cortical layers and resembled columns found in the adult cortex. In developing somatosensory cortex, domains were smaller than, and distinct from, the barrels, which represent sensory input from a single vibrissa. The neurons within each domain were coupled by gap junctions. Thus, nonsynaptic communication during cortical development defines discrete multicellular patterns that could presage adult functional architecture.

In mammalian neocortex, local circuits are preferentially organized in a radial direction, forming a modular architecture of columnar units (*1*). At least two possible developmental mechanisms, not mutually exclusive, could generate cortical columns. By analogy with the formation of ocular dominance stripes or clustered horizontal connections (*2*), columns could arise by activity-dependent formation, selection, or enhancement of connections in the vertical dimension. A different explanation—the "radial unit" hypothesis—has been formulated by Rakic (*3*). According to this theory, polyclones of developing neurons migrate to the cortex along radial glial fibers and, based on their migratory history, form radial units, which subsequently differentiate into adult columns. Both hypotheses require the presence of some type of mechanism, early in cortical development, to inform neurons that they are members of a distinct radial group. By visualizing patterns of multicellular activity, we have revealed the existence of one such possible mechanism.

To study the behavior of cortical networks as local microcircuits emerge, we used optical recordings with the Ca^{2+}-sensitive indicator fura-2 (*4*) in slices of developing rat cortex. Because neuronal activity is associated with presynaptic and postsynaptic Ca^{2+} influx (*5*), imaging of neuronal populations labeled with Ca^{2+}-sensitive indicators offers a sensitive method for optical recording of both suprathreshold and subthreshold events. Fura-2 can be used in slices of developing neocortex to reveal transmitter-induced Ca^{2+} changes in neurons (*6*); we have applied this approach to visualize multicellular patterns of spontaneous activity in these slices.

Optical recordings (*7*) were carried out in 12 coronal (across layers) and 12 tangential (parallel to the layers) slices obtained from somatosensory, visual, and frontal cortices of rats during postnatal days (PND) 0

Table 1. Total number of domains recorded and the instances of recurrences in 24 tangential (t) and coronal (c) cortical slices from PND 0 to 7 rats. PND 0 is the day of birth.

Age (PND), orientation	Number of domains	Recording time (s)	Number of recurrences
4, c	61	9596	16
5, c	38	8018	2
5, c	37	8008	6
4, c	37	5604	5
4, t	35	5876	3
5, t	35	7928	9
5, c	35	7216	3
3, c	34	10624	3
5, t	33	1200	3
4, c	27	4808	8
5, t	18	4800	1
4, t	16	1220	1
6, c	16	6192	0
4, c	15	3504	0
0, c	15	1396	0
5, t	13	8052	0
6, t	11	2812	1
6, t	8	2808	3
1, c	8	800	0
5, t	7	4472	0
6, t	5	4408	0
5, t	5	2576	0
1, c	5	4088	0
7, t	3	2300	0

Department of Neurobiology, Box 3209, Duke University Medical Center, Durham, NC 27710.

*To whom correspondence should be addressed.

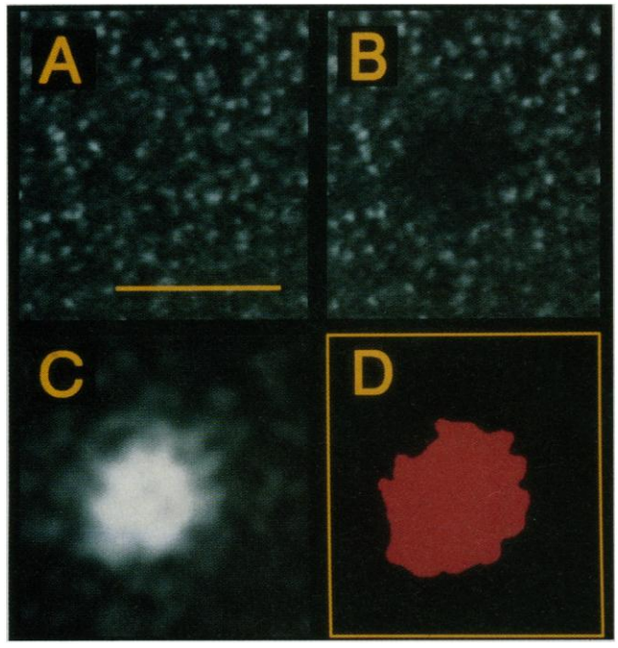

Fig. 1. Image processing techniques used to define neuronal domains. (**A**) Fura-2 fluorescence image (385-nm excitation) at time 0 of a tangential slice of PND 4 rat somatosensory cortex. Scale bar, 100 μm. (**B**) Fura-2 image 4 s later. (**C**) Subtracted image (A − B) after smoothing with a 15 by 15 pixel Gaussian kernel. The subtraction of the two images highlights areas that change in fluorescence as a consequence of increasing their $[Ca^{2+}]_i$. (**D**) Area of the neuronal domain after background subtraction and application of a binary threshold.

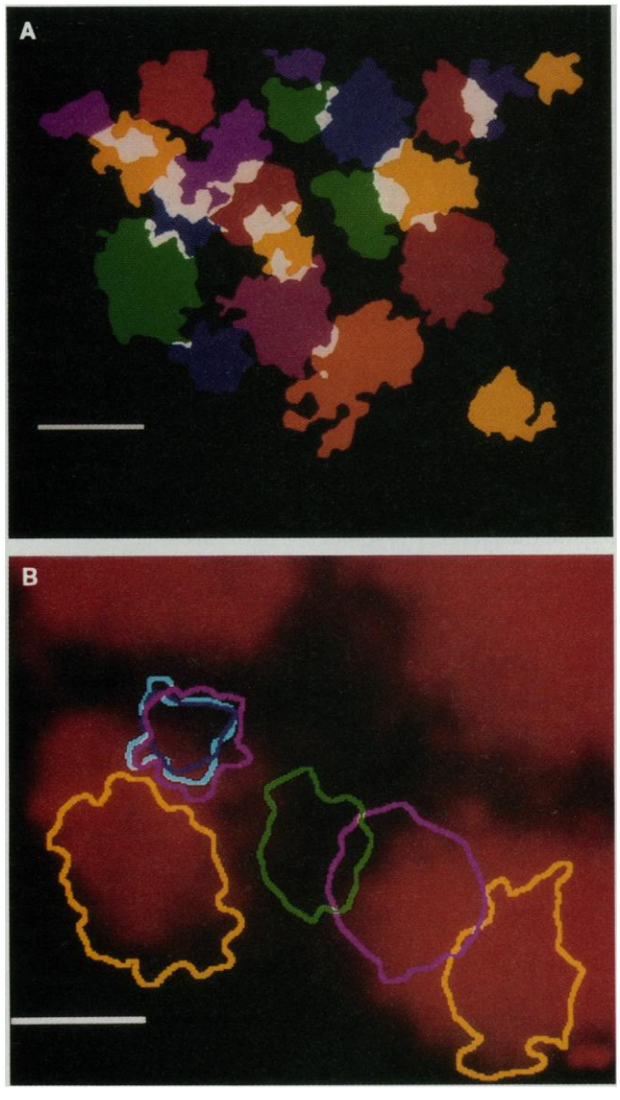

Fig. 2. (**A**) Map of neuronal domains in a tangential slice of PND 4 somatosensory cortex. Twenty-one domains, recorded over a period of 30 min, have been image-processed, color coded, and superimposed in a map. White indicates areas of overlap between two or more domains. Domains cover much of the slice with little overlap with neighboring domains. Scale bar, 100 μm. (**B**) Relation between neuronal domains and thalamocortical afferents in a tangential slice. Superimposed map of the outlines of seven neuronal domains in a PND 5 layer 4 tangential slice in which the thalamocortical afferents (barrels) have been labeled by a thalamic injection of TRITC on PND 1. Barrels are red in the figure. All domains are smaller than an individual barrel. One domain (green outline) clearly falls outside the barrels, and the rest are primarily confined to single barrels and subdivide each barrel into several coactive zones. One domain repeats itself three times (light blue, dark blue, and pink) at a very similar location during the course of the experiment. Scale bar, 50 μm.

to 7 (Table 1). These ages correspond to the critical period of development of the primary somatosensory cortex in rats (8). When large areas of cortex (~1 mm^2) were imaged, we observed discrete groups of cells that spontaneously changed their internal free Ca^{2+} concentration ($[Ca^{2+}]_i$) in synchrony, thereby defining coactive domains (Fig. 1). Domains appeared spontaneously in every slice at random intervals, with an average of 4 min between individual occurrences (517 domains in 32 hours of optical recordings). The spontaneous activation of any one zone had no relation to the activation of other nearby domains. The resulting elevations of $[Ca^{2+}]_i$ ranged from approximately 100 to 350 nM (from 50 ± 9 to 206 ± 24 nM, mean ± SD, $n = 43$), rising to peak levels in less than 1 s and persisting for 4 to 20 s (10.9 ± 4.9 s, $n = 43$). In tangential slices that included layers 2/3 to 4, these roughly circular domains, approximately 75 μm in diameter, had areas of 4426 ± 4105 μm^2 ($n = 128$). Each domain had discrete borders and contained 5 to 50 coactive cells in the plane of focus; fluorescence from out-of-focus cells also changed in synchrony with the visible cells. We found no differences in the size, shape, or frequency of domains in different cortical areas.

Oscillations and transient elevations in Ca^{2+} concentrations with complex spatiotemporal characteristics have been described in glial cultures (9). Several lines of evidence, however, indicate that the domains described here consist of neurons. First, the morphologies of the fura-2–labeled cells that formed the domains were clearly neuronal, as evidenced (in coronal sections) by their apical dendrites and large cell bodies (6). Second, differentiated astrocytes are uncommon during the first postnatal days in rat cortex (*10*). Finally, five additional optical recording experi-

Table 2. Computer simulation of four maps obtained from tangential slices from PND 4 to 6 rat cortex. We simulated experiments on a Macintosh IIci by assigning random positions to the domains and placing them in an area equal to the minimum rectangle that enclosed the actual map. The actual maps occupied 35 to 48% of rectangle area. Overlap was defined as the percentage of the area of the map occupied by more than one domain. The overlap of the random maps followed a Gaussian distribution. The first experiment (4, t) is the map illustrated in Fig. 2A.

Age (PND), orientation	Overlap (%) actual map	Overlap (%) random maps (mean ± SD, *n*)	*P* <
4, t	9.5	26.8 ± 5.4, $n = 1006$	0.001
5, t	4.6	19.8 ± 7.6, $n = 3129$	0.05
6, t	10.2	24.5 ± 6.2, $n = 5655$	0.05
6, t	7.8	20.6 ± 6.5, $n = 2726$	0.05

ments were done in slices in which neurons had been retrogradely labeled by injections of fluorescent microspheres (*11*) in the contralateral cortex. In these recordings, retrogradely labeled neurons exhibited spontaneous $[Ca^{2+}]_i$ transients and belonged to domains.

When all the domains obtained from a tangential slice were superimposed, they covered the surface of the slice and formed maps (Fig. 2A). In these maps, domains abutted each other with little overlap, giving the map a highly organized appearance. To determine whether the spatial organization of maps could result from spatially random events, we performed computer simulations of four experiments (Table 2). We first determined the amount of overlap between domains in the real map. Each domain was then assigned a random position and the amount of overlap in the "random maps" was calculated. In all cases, the average overlap of the random maps was significantly different from that of the real maps ($P < 0.05$); in the experiment in Fig. 2A, the actual degree of overlap did not occur in any of the 1006 random maps generated. Thus, the spatial distribution of domains is not random but probably relates to some underlying organization in the slice. Consistent with this idea, 64 of 517 domains reappeared at the site of a previous domain and covered 70 to 100% of its area. These recurrences were relatively infrequent and the interval between them was highly irregular (Table 1). In this way, they differ markedly from the relatively regular waves of activity described in fetal retina (*12*).

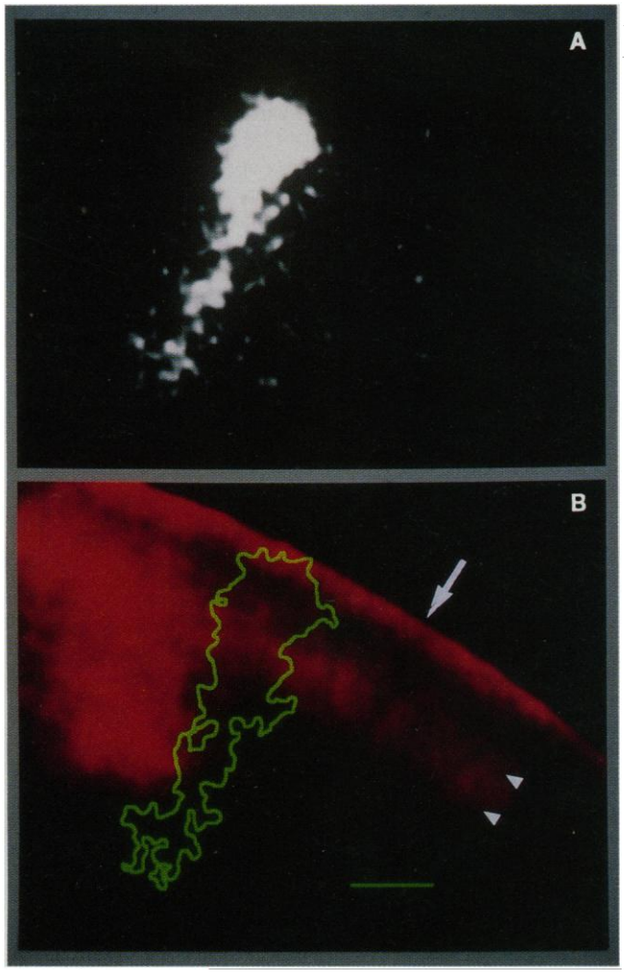

Fig. 3. Columnar domain in a coronal slice. (**A**) Image resulting from subtracting two 385-nm fluorescent images, 4 s apart, in a coronal slice of PND 3 rat somatosensory cortex. (**B**) Superposition of the outline of this domain with the anterograde staining of thalamocortical afferents. Pial surface indicated by arrow. Tetramethylrhodamine isothiocyanate was injected at PND 1 in the ventrobasal thalamus and stains three red bands in the cortex: layer 1 (superficial band on top), layer 4 (middle band, between arrowheads), and layer 6 (visible at the bottom left of the domain). This domain extends throughout the radial thickness of the cortex. Scale bar, 100 μm.

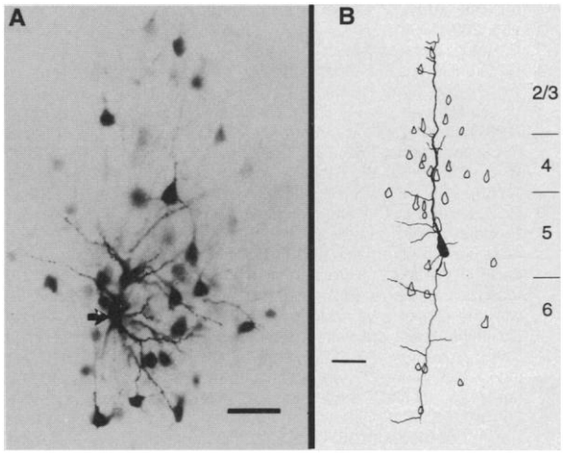

Fig. 4. Coupled clusters of neurons in developing cortex. (**A**) High-magnification view of a cluster of coupled neurons in a coronal slice of PND 7 cortex. The darker cell, marked with an arrow, was injected intracellularly with Neurobiotin, which stains its soma and dendrites. Nearby coupled neurons have more faintly stained cell bodies and processes. Scale bar, 50 μm. (**B**) Camera lucida reconstruction of all the neurons in a Neurobiotin-labeled cluster from a coronal slice of PND 5 rat cortex. Neurons in this cluster are distributed in a column extending from layer 2 to layer 6. Scale bar, 50 μm.

Because the tangential organization of the domains resembled cortical maps, we explored the possible relations between these coactive regions and known features of cortical architecture. A prominent feature of the primary sensory cortex is the segregation of thalamocortical afferents into discrete territories (*13*). To test whether domains were related to patterns of thalamic innervation, we combined fura-2 imaging with fluorescent anterograde labeling (*14*) of thalamocortical afferents in nine tangential slices of somatosensory cortex. Tetramethylrhodamine isothiocyanate (TRITC) was injected into the ventrobasal nucleus of the thalamus of PND 1 rats. Tangential slices through layer 4 prepared at PND's 4 to 6 produced the expected pattern of barrels; this enabled us to simultaneously image domains and barrels in the same slice (Fig. 2B). Individual domains were invariably smaller than single barrels (average barrel area, 42,765 ± 14,483 μm^2; range, 15,830 to 79,652 μm^2; $n = 14$; average domain area, 4,426 ± 4,105 μm^2; range, 589 to 12,952 μm^2; $n = 128$) and were located both inside (34 out of 78) and outside (44 out of 78) the barrels, subdividing them into several coactive zones. The relation of the domains to the borders of barrels was difficult to establish because of the lack of complete segregation of the afferents at these ages (*15*).

In coronal slices, domains were columnar. Nine domains (out of 219) clearly extended from layer 6 to layer 1 and spanned the entire thickness of the cortex (Fig. 3). The remaining domains were ovoid, approximately 50 by 200 μm, and their longer axes were oriented radially, crossing at least two layers. Of these 210 remaining domains, 62 were centered in layer 2/3, 133 in layer 4, and 15 in layers 5

and 6. Because the loading of neurons by fura-2 is poor in the lower layers (6), domains in these layers were more difficult to resolve (16). The shape of the coronal domains strongly suggests the columnar units of visual and somatosensory cortex (1) and the proposed radial units associated with radial glial fibers (3).

To elucidate the mechanisms responsible for the coactivation of cells within a domain, we imaged slices perfused with the Na^+ channel blocker tetrodotoxin (TTX), which prevents Na^+-based action potentials. In previous control experiments, 1 μM TTX blocked all stimulus-evoked synaptic activity and all synaptically induced Ca^{2+} influx. In all cases (13 slices), 5 μM TTX failed to prevent the appearance of domains, indicating that the coactivation of neurons in domains did not require Na^+-based action potentials or the synaptic events they could trigger. This persistence of the domains in TTX suggested that cells within a domain might be coupled by gap junctions because gap junctions are permeable to small ions, including Ca^{2+} (17). We probed for the presence of gap junctions by intracellular injections of Neurobiotin (biotin ethylenediamine, Vector Labs), a small diffusible tracer that labels coupled neurons in the retina (18). In 14 out of 24 cases, injection of a single cell in coronal slices from PND 5 to 10 somatosensory cortex resulted in labeling of a cluster of 15 to 78 cells (35 ± 17, n = 14) located in the immediate vicinity of the injected cell (Fig. 4A). Control injections into the extracellular space produced no labeling. Most labeled cells had pyramidal-shaped cell bodies and apical dendrites; none of the labeled cells resembled glia. Clusters were ovoid (124 ± 35 by 299 ± 155 μm, n = 14), radially oriented, and spanned several layers. In five of seven cases at PND 5, clusters formed columns stretching from layer 6 to the top of layer 2 (Fig. 4B). In all clusters the dendrites of the injected cell intersected cell bodies or apical dendrites of distantly labeled cells, suggesting dendrodendritic or dendro-somatic coupling. The spatial similarities between the Neurobiotin clusters and the optically recorded domains strongly suggest that both methods reveal the same organization.

The existence of coupled cells in cortical slices has been described in studies that used Lucifer yellow as a tracer. Injections with microelectrodes (19) showed small numbers of coupled cells (three to seven) in neonatal rat and guinea pig cortex, whereas injections with whole-cell electrodes revealed clusters of coupled neuroblasts in the embryonic ventricular zone that disappeared in the more mature cortical plate (20). Our experiments with microelectrode injections of Neurobiotin revealed extensive coupling in all cortical layers throughout the first two postnatal weeks. The differences from previous studies are probably attributable to the different tracers used: Neurobiotin (molecular weight 323) is smaller than Lucifer yellow (molecular weight 457) and should cross different classes of gap junctions more readily.

Cellular communication by means of gap junctions is found during pattern formation in vertebrate and invertebrate development (21). How this coupling is established and regulated in the mammalian neocortex remains unclear. During early cortical development, synapse number is low (22), synaptic activity is sparse, and neurons are difficult to stimulate (23). Gap junctions could enable developing cortical neurons to interact by a more direct, nonsynaptic mechanism. Our results indicate that this coupling underlies the coactivation of neurons within a domain. Because domains have similar sizes and discrete borders, they may represent modular functional units in developing cortex (24). Their radial arrangement is consistent with the radial unit hypothesis (3). In addition, although cells in a domain seem to behave independently of conventional synaptic transmission, their electrical coupling could influence subsequent synaptic rearrangements. If synapses are formed, retained, or modified by activity-dependent mechanisms (2, 25), selective synapse formation could occur among members of a domain, resulting in an adult column. Thus, the patterning of neonatal cortex into coupled neuronal domains may represent a developmental blueprint for the adult functional architecture.

REFERENCES AND NOTES

1. R. Lorente de Nó, in *Physiology of the Nervous System*, J. F. Fulton, Ed. (Oxford Univ. Press, New York, ed. 3, 1949), pp. 274–301; D. H. Hubel and T. N. Wiesel, *Proc. R. Soc. London Ser. B* **198**, 1 (1977); V. B. Mountcastle, in *The Mindful Brain*, F. O. Schmitt, Ed. (MIT Press, Cambridge, MA, 1978), pp. 7–51.
2. T. N. Wiesel, *Nature* **299**, 583 (1982); E. M. Callaway and L. C. Katz, *Proc. Natl. Acad. Sci. U.S.A.* **88**, 745 (1991); S. Löwel and W. Singer, *Science* **255**, 209 (1992).
3. P. Rakic, *Science* **241**, 170 (1988).
4. G. Grynkiewicz, M. Poenie, R. Y. Tsien, *J. Biol. Chem.* **260**, 3440 (1985).
5. V. Lev-Ram and A. Grinvald, *Biophys. J.* **52**, 571 (1987); D. W. Tank, M. Sugimori, J. A. Connor, R. R. Llinás, *Science* **242**, 773 (1988); K. R. Delaney, R. S. Zucker, D. W. Tank, *J. Neurosci.* **9**, 3558 (1989).
6. R. Yuste and L. C. Katz, *Neuron* **6**, 333 (1991).
7. Preparation of brain slices and optical recording were performed as described (6). Tangential slices (300 μm thick) were cut from primary somatosensory cortex of PND 0 to 7 Long-Evans rats with the use of a vibratome; coronal slices (400 μm thick) were cut with a special slicer [L. C. Katz, *J. Neurosci.* **7**, 1223 (1987)]. Slices were incubated in Mg^{2+}-free artificial cerebrospinal fluid (125 mM NaCl, 5 mM KCl, 1.25 mM KH_2PO_4, 26 mM $NaHCO_3$, 10 mM D-glucose, 3.1 mM $CaCl_2$, bubbled with 95% O_2, 5% CO_2) containing 10 μM fura-2/AM (Molecular Probes) and imaged at room temperature on an inverted microscope (Zeiss IM35) with an intensified charge-coupled-device camera (Hamamatsu) coupled to an image processor (Imaging Technologies Series 151). Background-subtracted images at a single excitation wavelength (385 nm) were collected every 1 to 10 s and stored with an optical disk recorder (Panasonic 2028F); each image was the average of 16 frames. For approximate estimates of $[Ca^{2+}]_i$, recordings at two wavelengths (350 and 385 nm) were performed and analyzed as described (6). For domain detection, sequential images were subtracted from each other. Images were then processed on a Macintosh IIfx with the program Image (NIH). Subtracted images were convolved with the use of a 15 by 15 pixel Gaussian kernel, the average background noise (mean ± 2 SD) was subtracted, and the resulting image was made binary. The border of contiguous positive areas was drawn to define a domain. Maps of domains were obtained by superimposing domains from the same optical recording sequence.
8. H. Van der Loos and T. A. Woolsey, *Science* **179**, 395 (1973).
9. A. H. Cornell-Bell, S. M. Finkbeiner, M. S. Cooper, S. J. Smith, *ibid.* **247**, 470 (1990); A. M. Jensen and S. Y. Chiu, *J. Neurosci.* **10**, 1165 (1990).
10. C. Kaur, E. A. Ling, W. C. Wong, *Acta Anat.* **136**, 204 (1989); J. P. Misson, T. Takahashi, V. S. Caviness, *Glia* **4**, 138 (1991).
11. L. C. Katz, A. Burkhalter, W. J. Dreyer, *Nature* **310**, 498 (1984).
12. M. Meister, R. O. L. Wong, D. A. Baylor, C. J. Shatz, *Science* **252**, 939 (1991).
13. D. H. Hubel, T. N. Wiesel, S. LeVay, *Philos. Trans. R. Soc. London Ser. B* **178**, 377 (1977); T. A. Woolsey and H. Van der Loos, *Brain Res.* **17**, 205 (1970).
14. L. C. Katz, C. D. Gilbert, T. N. Wiesel, *J. Neurosci.* **9**, 1389 (1989).
15. The thalamocortical afferents are not totally segregated until after PND 7. Because of age-dependent limitations in the loading of fura-2 (6), we could not perform these optical recordings later than PND 7.
16. The small number of columnar domains that spanned the entire thickness of the cortex could also be explained by the plane of section: imaging of an entire column may only be possible if slices are cut at a plane closely parallel to the circuitry. In all other cases, even a slightly oblique section through a column would produce an ovoid. In agreement with this, some slices had a higher proportion of columnar domains.
17. J. C. Sáez, J. A. Connor, D. C. Spray, M. V. L. Bennett, *Proc. Natl. Acad. Sci. U.S.A.* **86**, 2708 (1989).
18. D. I. Vaney, *Neurosci. Lett.* **125**, 187 (1991). Neurons in coronal slices (400 μm thick) of rat somatosensory cortex were impaled intracellularly with glass microelectrodes (80- to 100-megohm resistance) filled with 15% Neurobiotin in 1 M KCl. The tracer was ejected iontophoretically with positive current pulses (200 ms; 0.3 nA) for 5 to 10 min. Slices were then fixed in 4% paraformaldehyde and resectioned at 75-μm thickness. The Neurobiotin was visualized with the avidin-biotin horseradish peroxidase method (Vector Labs) and diaminobenzidine (Sigma).
19. M. J. Gutnick and D. A. Prince, *Science* **211**, 67 (1981); B. W. Connors, L. S. Bernardo, D. A. Prince, *J. Neurosci.* **3**, 773 (1983).
20. J. J. Lo Turco and A. R. Kriegstein, *Science* **252**, 563 (1991).
21. S. C. Guthrie and N. B. Gilula, *Trends Neurosci.* **12**, 12 (1989).
22. M. Armstrong-James and R. Johnson, *Z. Zellforsch. Mikrosk. Anat.* **110**, 559 (1970); B. G. Cragg, *J. Comp. Neurol.* **160**, 147 (1975).
23. D. H. Hubel and T. N. Wiesel, *J. Neurophysiol.* **26**, 994 (1963); M. Armstrong-James, *J. Physiol.* **246**, 501 (1975).
24. Although we have not attempted to observe these domains in vivo, it is extremely unlikely that they represent a slice artifact. Domains occur whether

slices are prepared in the tangential or coronal plane. In addition, their regular spatial arrangement, repeatability at specific locations, and occurrence in virtually every slice strongly suggest that they are not artifacts. Furthermore, optical recordings were done directly on a glass cover slip; no netting or other support with a regular geometry was used at any time. Finally, results on the specific pharmacology of domains do not support a slice artifact; whereas TTX, a Na^+ channel blocker, does not block domains, octanol and halothane, which are gap junction blockers, reversibly prevent the occurrence of domains.

25. D. O. Hebb, *The Organization of Behavior* (Wiley, New York, 1949), p. 62; G. S. Stent, *Proc. Natl. Acad. Sci. U.S.A.* **70**, 997 (1973).

26. We thank D. Nelson for programming the simulations; E. Callaway, D. Purves, and T. Wiesel for comments on the manuscript; P. Peirce for photography; and C. Gutman for technical assistance. Supported by a Rockefeller University graduate fellowship (R.Y.), by NIH grants MH15177 (A.P.) and EY07960, and by an L. P. Markey Charitable Trust Scholar's Award (L.C.K.).

8 November 1991; accepted 3 June 1992

Chloride-Dependent Cation Conductance Activated During Cellular Shrinkage

Hsiao Chang Chan and Deborah J. Nelson*

A chloride (Cl^-)-dependent, nonselective cation conductance was activated during cellular shrinkage and inhibited during cellular swelling or by extracellular gadolinium. The shrinking-induced, nonselective cation conductance and the swelling-induced anion conductance appear to function in the regulation of cell volume in airway epithelia. The shrinking-induced cation conductance had an unusual dependence on Cl^-: partial replacement of extracellular Cl^- with aspartate reduced the magnitude of the shrinking-enhanced current without accompanying changes in the reversal potential. The Cl^- dependence of the nonselective cation conductance could provide a mechanism that tightly regulates Cl^- secretion and sodium reabsorption in cells under osmotic stress.

Exposure of cells to anisosmotic (hypotonic or hypertonic) media drives water into or out of the cell, resulting in acute swelling or shrinking (*1*). Many cells respond to these volume changes by modulating membrane conductance pathways as well as metabolic pathways that alter the concentration of intracellular solutes, thereby restoring cell volume to its original value. The cellular regulatory processes elicited after osmotic swelling or shrinkage are termed "regulatory volume decrease" (RVD) and "regulatory volume increase" (RVI), respectively. Regulation of cell volume is critical in certain pathological states such as ischemia and disturbances in cellular metabolism that are accompanied by swelling of cells. Even under physiological conditions, cells in the renal medulla and the intestine are subjected to osmotic stress induced by increased osmolarity in the extracellular fluid and the circulating blood plasma. Most actively transporting epithelial cells also experience osmotic variations as a result of the accumulation of osmotically active solutes within the cells and therefore must adapt to survive in environments both higher and lower in osmolarity than that of plasma.

Ion channels have been reported to participate in cell volume regulation by selectively governing the movement of ions into and out of cells. Both K^+ and Cl^- channels can be activated after a hypo-osmotic challenge, thereby initiating RVD. The increase in K^+ or Cl^- conductances, or both, results in the loss of KCl from the cell and a parallel reduction in cell volume. The extent of the reduction in cell volume is limited by the maintenance of a cellular membrane potential that favors the efflux of both ions (*2*, *3*). The activation of ion channels in response to a hyperosmotic challenge has not been demonstrated, although the participation of Na^+ or nonselective cation channels in RVI has been proposed (*4*). This study demonstrates the activation of a Cl^--dependent, nonselective cation conductance during cellular shrinkage. Cultured, dissociated human airway epithelial cells were studied with the whole-cell patch-clamp technique (*5*).

Activation of a current with a relatively linear current-voltage (*I-V*) relation occurred after exposure of a cell to a hypertonic bathing solution (*6*). The magnitude of the current increased as the osmotic pressure difference across the cell membrane was increased by the addition of sucrose to the external solution, suggesting that the current was associated with cellular shrinkage (Fig. 1). Current activation was reversed by decreasing the osmolarity of the bathing solution so that it was hypo-osmotic to the intracellular (pipette) solution. Isotonicity between cell interior and exterior was obtained when the bathing solution was made hypotonic by 30 mOsM to the intracellular solution, as determined by the absence of current activation under these conditions. Representative whole-cell currents after cellular shrinkage in response to step changes in membrane potential between −110 and +100 mV can be seen in Fig. 2, A and B. In these experiments, Na^+ and Cl^- were the major permeant ionic species, and current separation was made on the basis of shifts in reversal potential (*7*). The equilibrium potentials for a perfectly cation- or anion-selective conductance were +31 and −31 mV, respectively. Shrinking-induced current activation was associated with a depolarizing shift in current reversal potential (+26 ± 1 mV, n = 14) close to the predicted equilibrium potential for Na^+, indicating that the current was predominantly cation-selective.

The cation to anion selectivity was determined for the shrinking-activated conductance from current reversal potentials obtained when NaCl in the intracellular solution was substituted in various amounts with

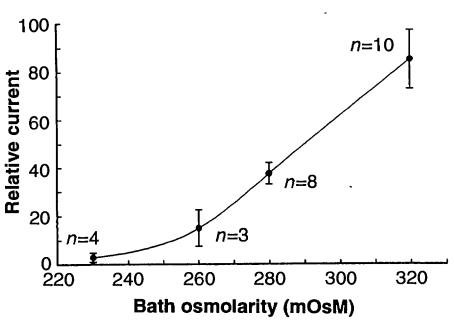

Fig. 1. Relation between whole-cell current (at 50 mV) and bath osmolarity. Experiments were performed on cultured, dissociated human airway epithelial cells with the use of the whole-cell patch-clamp technique. The pipette solution contained 40 mM NaCl, 100 mM NMDG-aspartate, 10 mM Hepes, 5 mM EGTA, 0.5 mM $CaCl_2$, and 1 mM $MgCl_2$, pH 7.2. The bath solution contained 140 mM NaCl, 10 mM Hepes, 2 mM $CaCl_2$, and 1 mM $MgCl_2$, pH 7.2. Extracellular solutions were made hypertonic by the addition of sucrose (standard bathing solution osmolarity was 280 mOsM). The relative current magnitude was determined as the ratio of the current for a test solution osmolarity to the average current value recorded in cells exposed to a bathing solution of 230 mOsM ($I_{\text{test osmolarity}}/I_{230\ \text{mOsM}}$). The mean current amplitude in cells exposed to the 230-mOsM bathing solution was 61 ± 7 pA at +50 mV (n = 4). Current magnitudes recorded under hypotonic conditions (bath solution <280 mOsM) were obtained after the cells had been exposed to hypertonic bathing solutions (solutions ≥280 mOsM). Inactivation of the shrinking-induced currents occurred at about 250 mOsM, as deduced from extrapolation of the curve (which corresponds to a difference of 30 mOsM between pipette and bath solutions).

Department of Medicine and Department of Neurology, University of Chicago, Chicago, IL 60637.

*To whom correspondence should be addressed.